

Free energy surface of ST2 water near the liquid-liquid phase transition

Peter H. Poole, Richard K. Bowles, Ivan Saika-Voivod, and Francesco Sciortino

Citation: *J. Chem. Phys.* **138**, 034505 (2013); doi: 10.1063/1.4775738

View online: <http://dx.doi.org/10.1063/1.4775738>

View Table of Contents: <http://jcp.aip.org/resource/1/JCPSA6/v138/i3>

Published by the [American Institute of Physics](#).

Additional information on *J. Chem. Phys.*

Journal Homepage: <http://jcp.aip.org/>

Journal Information: http://jcp.aip.org/about/about_the_journal

Top downloads: http://jcp.aip.org/features/most_downloaded

Information for Authors: <http://jcp.aip.org/authors>

ADVERTISEMENT



Goodfellow
metals • ceramics • polymers • composites
70,000 products
450 different materials
small quantities fast

www.goodfellowusa.com

Free energy surface of ST2 water near the liquid-liquid phase transition

Peter H. Poole,¹ Richard K. Bowles,² Ivan Saika-Voivod,³ and Francesco Sciortino⁴

¹*Department of Physics, St. Francis Xavier University, Antigonish, Nova Scotia B2G 2W5, Canada*

²*Department of Chemistry, University of Saskatchewan, Saskatoon, Saskatchewan S7N 5C9, Canada*

³*Department of Physics and Physical Oceanography, Memorial University of Newfoundland, St. John's, Newfoundland A1B 3X7, Canada*

⁴*Dipartimento di Fisica, Università di Roma La Sapienza, Piazzale A. Moro 5, 00185 Roma, Italy*

(Received 23 November 2012; accepted 27 December 2012; published online 17 January 2013)

We carry out umbrella sampling Monte Carlo simulations to evaluate the free energy surface of the ST2 model of water as a function of two order parameters, the density and a bond-orientational order parameter. We approximate the long-range electrostatic interactions of the ST2 model using the reaction-field method. We focus on state points in the vicinity of the liquid-liquid critical point proposed for this model in earlier work. At temperatures below the predicted critical temperature we find two basins in the free energy surface, both of which have liquid-like bond orientational order, but differing in density. The pressure and temperature dependence of the shape of the free energy surface is consistent with the assignment of these two basins to the distinct low density and high density liquid phases previously predicted to occur in ST2 water. © 2013 American Institute of Physics. [<http://dx.doi.org/10.1063/1.4775738>]

I. INTRODUCTION

In 1992, the results of a computer simulation study of the ST2 model¹ of water were used to propose that a liquid-liquid phase transition (LLPT) occurs in supercooled water.² Below the critical temperature T_c for the proposed LLPT, two distinct phases of water, the low density liquid (LDL) and high density liquid (HDL) phases are separated by a first-order phase transition. The predicted phase diagram for the ST2 model in the plane of temperature T and pressure P in the vicinity of the critical point is shown in Fig. 1.

An appealing feature of the LLPT proposal is that it simultaneously accounts for (a) the unusual thermodynamic behavior of liquid water in the supercooled region, and (b) the occurrence of two distinct forms of amorphous solid water in the glassy regime.^{3,4} Evidence for a LLPT has been reported in a number of simulation studies of water and water-like systems; see, e.g., Refs. 5–11. Experimentally, a LLPT has yet to be decisively confirmed in supercooled water, and efforts to resolve this question in the laboratory continue.^{12–15} The predicted location of the critical point in the supercooled regime is challenging to study in experiments because of rapid ice crystallization. In simulations, this problem is avoided when the liquid can be studied on a time scale that is long relative to the liquid-state relaxation time, but short compared to crystal nucleation times.

Recently, Limmer and Chandler¹⁶ have challenged the LLPT hypothesis. Using umbrella sampling Monte Carlo (MC) simulations of two water models (mW¹⁷ and ST2 water), Ref. 16 presents results for the free energy surface $F(\rho, Q_6)$ of the liquid as a function of two order parameters, the density ρ , and a bond-orientational order parameter Q_6 . Q_6 is a bulk order parameter used to distinguish crystalline configurations from liquid or amorphous solid states of a system. Values of Q_6 approaching zero correspond to disordered states,

while larger values of Q_6 indicate greater degrees of crystalline order. The detailed definition of Q_6 is given in Eqs. (1)–(3) of Ref. 16, and is based on an analysis of the orientation of local molecular environments (i.e., a molecule and its nearest neighbors) in terms of spherical harmonics, as originally proposed by Steinhardt *et al.*¹⁸ In the present work, we use the same definition of Q_6 as given in Ref. 16.

It has long been appreciated that the density of the proposed LDL and HDL phases must be different. The innovation of Ref. 16 is that by examining the dependence of $F(\rho, Q_6)$ on Q_6 , Limmer and Chandler¹⁶ address the relationship of the metastable liquid phase to the ordered crystalline ice phases. If a LLPT occurs in a simulation model, then under appropriate conditions of T and P , two distinct free energy basins should be observed in $F(\rho, Q_6)$ in the low- Q_6 (i.e., liquid-like) regime. For both the mW and ST2 water models, Ref. 16 reports that only one liquid-like free energy basin is found in $F(\rho, Q_6)$, including, in the case of ST2 water, at conditions below the proposed critical temperature of the LLPT. Limmer and Chandler¹⁶ conclude that phenomena previously interpreted as evidence for a LLPT are in fact due to the liquid-to-crystal phase transition.

Since the publication of Ref. 16, Liu *et al.*¹⁹ have reported on their own evaluation of the free energy surface $F(\rho, Q_6)$ found from umbrella sampling MC simulations of ST2 water. Although they employ methods similar to those used in Ref. 16, Liu *et al.*¹⁹ report a very different result: the observation of two distinct liquid free energy basins in $F(\rho, Q_6)$, with properties consistent with the LLPT hypothesis. The results of Ref. 19 are also consistent with an earlier study by the same group reporting the free energy of ST2 water as a function of ρ only.²⁰

The precise reasons for the difference between the results of Refs. 16 and 19 for $F(\rho, Q_6)$ remain unclear. Among the differences in the approaches used in these two works, we

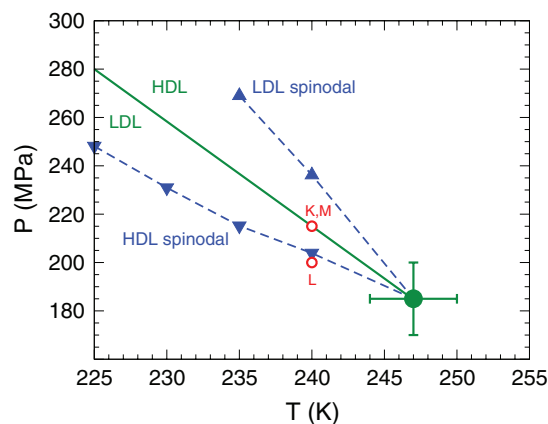


FIG. 1. Phase behavior of the ST2-RF model predicted from previous work using $N = 1728$ molecular dynamics simulations. Shown are the estimated locations of the critical point (green circle) and the LDL-HDL coexistence line near the critical point (green line). In Ref. 24, the Clapeyron slope m of the coexistence line near the critical point is estimated based on a mixture-model analysis of $N = 1728$ molecular dynamics simulations. The estimate for the coexistence line shown here is simply a straight line of slope m emanating from the critical point. Thus, the error bars associated with the critical point also apply to the coexistence line drawn here. Estimates for the HDL spinodal (downward triangles) and LDL spinodal (upward triangles) are also shown.⁶ Red circles locate the state points at which we carry out series K, L, and M of the present work.

note two. First, Limmer and Chandler¹⁶ present results for $F(\rho, Q_6)$ at various pressures as determined at one temperature, $T = 235$ K, which is below but within error of the estimated critical temperature $T_c = 237 \pm 4$ K for the ST2 model when studied with Ewald summations.²⁰ Working this close to T_c may make it difficult to discern distinct liquid basins in the free energy surface within the statistical error. Liu *et al.*¹⁹ report results for a range of temperatures below T_c , from $T = 224$ to 235 K, and show that the distinction between the two liquid basins that they observe in $F(\rho, Q_6)$ becomes greater as T decreases below T_c .

Second, in both Refs. 16 and 19, the method of Ewald summation is used to approximate the long-range contributions to the electrostatic potential energy of the ST2 system. However, Liu *et al.*¹⁹ report that their Ewald summation method employs vacuum boundary conditions, whereas Limmer and Chandler¹⁶ use conducting boundary conditions. Liu *et al.*¹⁹ note some significant sensitivity in the behavior of their system as a function of these boundary condition choices. If and how these boundary conditions might affect the qualitative shape of the $F(\rho, Q_6)$ surface is incompletely understood.

In light of the conflicting results of Refs. 16 and 19, we present here a new evaluation of the free energy surface $F(\rho, Q_6)$ of ST2 water. In order to expand our understanding of the role of long-range interactions, we use a different approach to account for the electrostatic energy, namely, the reaction field method.²¹ Indeed, many of the previous studies of ST2 water that relate to the LLPT hypothesis were conducted using the reaction field method,^{5,6,22,23} including the work in which the occurrence of a LLPT was first proposed.² Furthermore, a recent umbrella sampling MC study of the ST2 model, using the reaction field method, showed that the shape of the free energy as a function of ρ was consistent with the LLPT

hypothesis.²² An explicit examination of the $F(\rho, Q_6)$ surface for the ST2 model with a reaction field treatment of the electrostatics is therefore warranted. In addition, we also study a range of temperatures and pressures in the vicinity of the proposed critical point, to examine their influence on the $F(\rho, Q_6)$ surface.

II. ST2 MODEL

We study the ST2 model of water proposed by Stillinger and Rahman.¹ The ST2 pair potential is a sum of a Lennard-Jones (LJ) interaction (centered on the O atom), and electrostatic interactions involving four tetrahedrally positioned charges. Our model parameters for the geometry and pair interactions of the ST2 water molecule are the same as those given in Ref. 1. The potential energy U of our system is given by

$$U = U_E + U_{LJ} + \Delta U_{LJ}, \quad (1)$$

where U_E and U_{LJ} are the respective electrostatic and LJ contributions. In our simulations, the LJ interaction is sharply cut off when the O–O distance r exceeds $R_c = 0.78$ nm, and the contribution from longer ranged LJ interactions is approximated by

$$\Delta U_{LJ} = -\frac{8\pi\epsilon\sigma^6\rho_n N}{3R_c^3}, \quad (2)$$

as described in the Appendix of Ref. 1. In Eq. (2), N is the number of molecules, ρ_n is the number density of molecules, and ϵ and σ are the respective energy and size parameters of the LJ potential.

To evaluate U_E , the electrostatic contributions to the potential energy, we adopt the treatment used in the study of ST2 water by Steinhauser; see Eqs. (5) and (6) of Ref. 21. In this approach, the electrostatic interactions of the ST2 model are evaluated directly up to $r = R_c$ using the original form given in Ref. 1, including the use of a “switching function” to preclude a divergence of the energy due to charge overlaps. The contribution of electrostatic interactions beyond R_c is then approximated using the reaction field method, in which the liquid beyond R_c is treated as a polarizable dielectric continuum. As in Ref. 21, we assume that the dielectric constant of the continuum liquid is $\epsilon_R = \infty$. To avoid a sharp discontinuity in the electrostatic interactions at R_c , a tapering function (described in Ref. 21) is used to smoothly reduce the electrostatic interaction between two molecules (both direct and reaction field contributions) to zero over the interval $0.95R_c < r < R_c$.

The evaluation of the pair interactions as described above is the same procedure that was used in a number of previous studies.^{2,5,6,22,24,25} For the remainder of this paper, we will refer to the reaction field version of ST2 described above as ST2-RF, to emphasize the difference between the present study and those works that have studied the ST2 model using an Ewald treatment of the electrostatics.^{16,19,20}

III. SIMULATION METHODS

Our aim is to evaluate the free energy surface $F(\rho, Q_6)$ for the ST2-RF model in the vicinity of the predicted LLPT for

this model. To define $F(\rho, Q_6)$, let $p(\rho, Q_6)$ be proportional to the equilibrium probability for a microstate of the system at fixed values of N , T , and P to have order parameter values ρ and Q_6 . The conditional Gibbs free energy $F(\rho, Q_6)$ is then defined by

$$F(\rho, Q_6) = -kT \ln p(\rho, Q_6) + F_0, \quad (3)$$

where F_0 is an (irrelevant) constant related to the normalization of p , and k is Boltzmann's constant.¹⁶

We also define the ‘‘contraction’’ of F with respect to Q_6 as

$$\bar{F}(\rho) = -kT \ln \left(\int_0^{Q_6^{\max}} dQ_6 \exp[-\beta F(\rho, Q_6)] \right), \quad (4)$$

where $\beta = 1/kT$.¹⁶ $\bar{F}(\rho)$ represents the free energy as a function of ρ that would be found from an ensemble of states in which Q_6 is free to vary between zero and Q_6^{\max} . In this work, we are concerned with the liquid-like range of Q_6 . As shown below, we find that setting $Q_6^{\max} = 0.09$ is sufficient to characterize $\bar{F}(\rho)$ for the liquid-like basins of the free energy surface.

Following the approach of Ref. 16, we use umbrella sampling MC simulations to evaluate $F(\rho, Q_6)$. We carry out MC simulations in the constant- (N, P, T) ensemble, and to implement umbrella sampling, we add a biasing potential

$$U_B = k_1(\rho - \rho^*)^2 + k_2(Q_6 - Q_6^*)^2 \quad (5)$$

to the system potential energy U in Eq. (1). The effect of U_B is to constrain a given simulation to sample configurations in the vicinity of chosen values of the order parameters $\rho = \rho^*$ and $Q_6 = Q_6^*$. In all our simulations, we fix $N = 216$, $k_1 = 1000kT \text{ (cm}^3/\text{g)}^2$, and $k_2 = 2000kT$.

Trial configurations for each Monte Carlo step (MCS) are generated as follows: First, we carry out a mini-trajectory of 10 unbiased (i.e., $U_B = 0$) constant- (N, P, T) MC moves, in which each move consists (on average) of $N - 1$ attempted rototranslational moves, and one attempted change of the system volume. The maximum size of the attempted rototranslational and volume changes are chosen to give MC acceptance ratios in the range 25%–40%, depending on the thermodynamic conditions. Next, the change in the biasing potential U_B is evaluated for the trial configuration resulting from the mini-trajectory, relative to the system configuration at the beginning of the mini-trajectory, to determine the acceptance or rejection of the trial configuration. This completes one MCS, and the procedure is then repeated.

In order to identify the T - P state points at which to conduct our runs, we use the location of the LLPT reported in previous work. Figure 1 shows the estimates for the critical point and coexistence line obtained from $N = 1728$ molecular dynamics simulations of the ST2-RF model. Of particular importance are the locations of the spinodal lines for the LDL and HDL phases. These spinodal lines demarcate the stability limits for each phase. Consequently, if liquid-liquid coexistence does indeed occur in the ST2-RF model, the $F(\rho, Q_6)$ surface will simultaneously exhibit two distinct liquid basins only for state points lying in the region between the HDL and LDL spinodals. It is in this region of states that we focus our simulations. To carry out our runs, we select pressures that lie

between or near to the HDL and LDL spinodals, and a temperature ($T = 240$ K) that is 7 K below the estimated critical temperature of $T_c = 247 \pm 3$ for the ST2-RF model.²⁴

We carry out three distinct series of runs. In the following, ‘‘series K’’ denotes the set of runs conducted at $T = 240$ K, $P = 215$ MPa, $Q_6^* = 0.05$, and equally spaced values of ρ^* from 0.93 to 1.15 g/cm³, separated by 0.01 g/cm³. ‘‘Series L’’ denotes runs conducted at $T = 240$ K, $P = 200$ MPa, $Q_6^* = 0.05$, and equally spaced values of ρ^* from 0.95 to 1.15 g/cm³, separated by 0.01 g/cm³. ‘‘Series M’’ denotes runs conducted at $T = 240$ K, $P = 215$ MPa, $Q_6^* = 0.09$, and $\rho^* = 0.95$ g/cm³. The state points in the T - P plane corresponding to series K, L, and M are identified in Fig. 1. For all distinct choices of (T, P, ρ^*, Q_6^*) in the above series, we conduct 10 separate runs, each initiated from independent starting configurations. The results presented here are thus based on an analysis of 450 independent runs.

All our runs are carried out for between 5×10^6 and 5×10^7 MCS. Using the second half of each run, we compute $f(t)$, the collective intermediate scattering function as a function of time t . We evaluate $f(t)$ at the lowest-wavenumber peak in the static structure factor for the O atoms, i.e., the so-called first sharp diffraction peak of molecular tetrahedral networks. As shown in Figs. 2 and 3, in all cases $f(t)$ decays to zero on a time scale which is short compared to the lengths of our runs. Hence, the system behaviour is consistent with liquid-like relaxation under all conditions simulated in this study. After

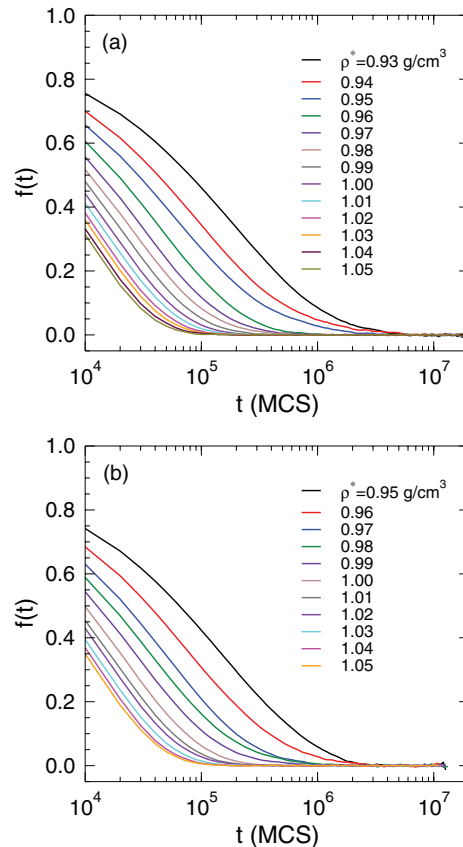


FIG. 2. Time dependence of the collective intermediate scattering function $f(t)$ for runs with various values of ρ^* in series (a) K and (b) L. Each curve is an average over 10 runs.

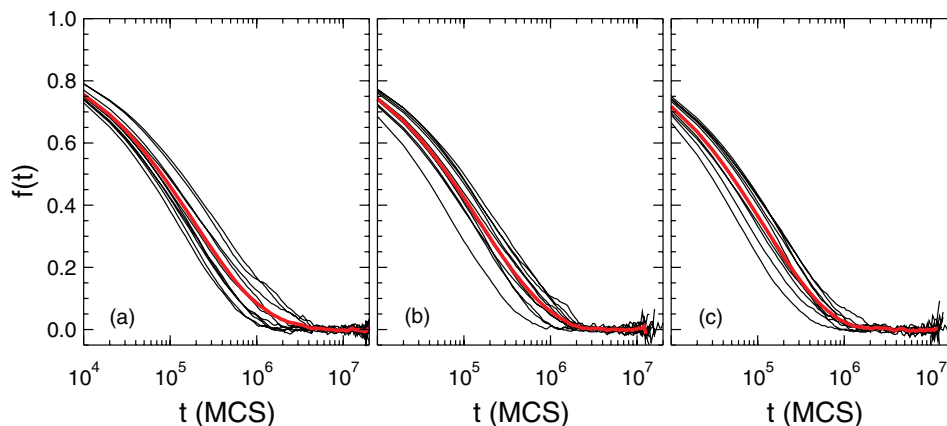


FIG. 3. Collective intermediate scattering function $f(t)$ for the lowest value of ρ^* from each series: (a) K, $\rho^* = 0.93 \text{ g/cm}^3$; (b) L, $\rho^* = 0.95 \text{ g/cm}^3$; and (c) M, $\rho^* = 0.95 \text{ g/cm}^3$. These are the most slowly relaxing runs used in our analysis. The black lines give $f(t)$ for each of the 10 independent runs conducted at the same values of (T, P, ρ^*, Q_6^*) , and the thick red line is their average.

averaging $f(t)$ over the 10 runs at each choice of (T, P, ρ^*, Q_6^*) , we estimate the alpha-relaxation time τ_α as the time at which $f(t) = e^{-1}$. As shown in Fig. 4, in all cases we find $\tau_\alpha < 2 \times 10^5 \text{ MCS}$. To account for equilibration, we then discard the results for $t < \tau_e$ of each run, where $\tau_e = 20\tau_\alpha$ or 10^4 MCS , whichever is larger. The resulting length τ_{run} of each production run that is used in our analysis is shown in Fig. 4, compared to the corresponding value of τ_α . In terms of τ_α , the lengths of our production runs range between $175\tau_\alpha$ and $4400\tau_\alpha$. As shown in Fig. 3, even our most slowly relaxing individual simulations are run for a time that is at least two orders of magnitude longer than the corresponding value of τ_α .

To estimate $F(\rho, Q_6)$, $\bar{F}(\rho)$, and the associated error, we use the multistage Bennet acceptance ratio (MBAR) method.²⁶ The MBAR method takes as input the time series of the order parameters (ρ and Q_6) and the system potential energy U , reweights the statistics obtained from each run to remove the effect of the biasing potential, and produces an optimal estimate of the desired free energy function at a specified value of T and P . The MBAR method also facilitates reweighting the configurations sampled during our runs with

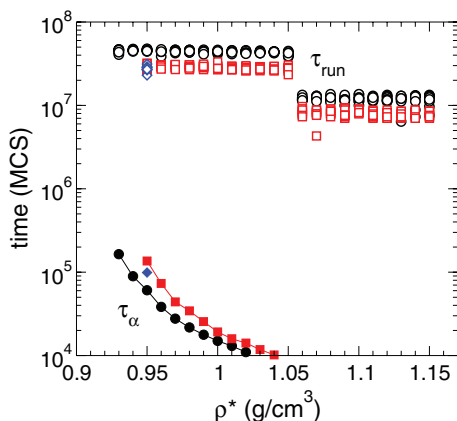


FIG. 4. Comparison of τ_α (filled symbols) and τ_{run} (open symbols) as a function of ρ^* for series K (circles), L (squares), and M (diamonds). Values of $\tau_\alpha < 10^4 \text{ MCS}$ are not shown.

respect to T and/or P , allowing the statistics from different state points to be combined to produce an estimate of $F(\rho, Q_6)$ or $\bar{F}(\rho)$ at T - P state points that lie near to the conditions at which we carry out our simulations.

For the purpose of estimating the free energy and its error using MBAR, we wish to consider only those configurations from our runs that are statistically independent. We assume that statistically independent configurations are separated by τ_α or 10^4 MCS , whichever is larger. All other configurations are ignored in our analysis. Note that in all our plots the indicated error is the error with respect to the minimum value of the estimated free energy, which in most cases is arbitrarily set to zero. Also, all error bars reported here represent one standard deviation of error.

IV. RESULTS

First, we compare the results obtained for $\bar{F}(\rho)$ at the two state points directly simulated in our runs. Series K and M are both conducted at $T = 240 \text{ K}$ and $P = 215 \text{ MPa}$, while series L is conducted at $T = 240 \text{ K}$ and $P = 200 \text{ MPa}$. The results for $\bar{F}(\rho)$ obtained using only series K and M, and that obtained using only series L are compared in Fig. 5. The shapes of both curves suggest the existence of two distinct free energy minima separated by an interval of thermodynamic instability with respect to ρ , as indicated by concave-down curvature of $\bar{F}(\rho)$. One minimum is centred near 0.9 g/cm^3 and the other near 1.05 g/cm^3 .

To check that the statistics we have gathered in series K and M are consistent with the results obtained from series L (and vice versa), we also show in Fig. 5 the result for $\bar{F}(\rho)$ found by reweighting our data from series K and M to $P = 200 \text{ MPa}$, and the result found by reweighting our data from series L to $P = 215 \text{ MPa}$. The reweighted results are in good agreement with the unweighted curves, confirming that both data sets have independently converged to equilibrium. In the remainder of this paper, all results shown for $\bar{F}(\rho)$ and $F(\rho, Q_6)$ are, therefore, obtained by combining the statistics from all three simulation series, K, L, and M.

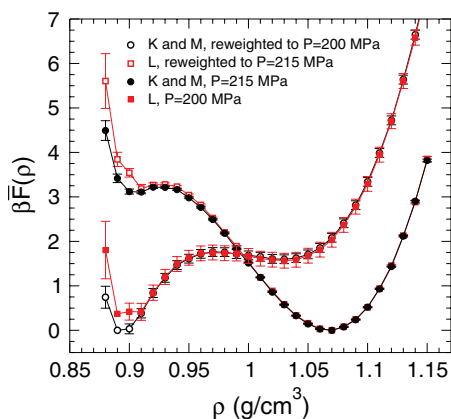


FIG. 5. Contracted free energy $\bar{F}(\rho)$ at $T = 240$ K, at two different pressures. The filled circles are obtained by analyzing series K and M at $P = 215$ MPa, the pressure at which these series are conducted; the open circles are obtained by reweighting these results to $P = 200$ MPa. The filled squares are obtained by analyzing series L at $P = 200$ MPa, the pressure at which this series is conducted; the open squares are obtained by reweighting these results to $P = 215$ MPa.

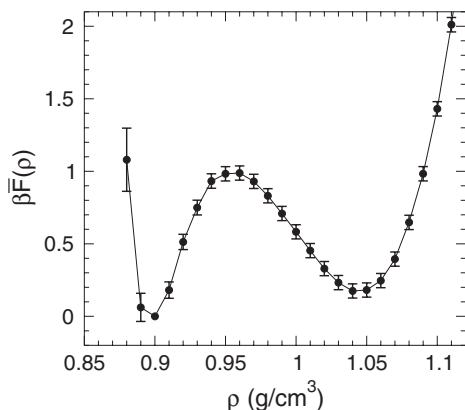


FIG. 6. Contracted free energy $\bar{F}(\rho)$ at $T = 240$ K and $P = 204.5$ MPa, obtained by combining all results from series K, L, and M.

In Fig. 6, we show $\bar{F}(\rho)$ at $T = 240$ K and $P = 204.5$ MPa, a pressure intermediate between those shown in Fig. 5. At this state point, $\bar{F}(\rho)$ clearly displays two distinct free energy minima, separated by a free energy barrier of approximately $1kT$, a typical value when T is close to T_c .

We next analyze the behavior of the free energy surface $F(\rho, Q_6)$. Figure 7 shows contour plots of $F(\rho, Q_6)$ at $T = 240$ K for three pressures from $P = 195$ to 230 MPa. The $F(\rho, Q_6)$ surface at $P = 204.5$ MPa simultaneously displays two free energy basins, each corresponding to a distinct metastable thermodynamic phase. The minima of both basins are located at liquid-like values of Q_6 in the range 0.05 – 0.065 . The shape of both basins shows that the phases they represent are locally stable with respect to fluctuations in both ρ and Q_6 . The stability of both phases with respect to Q_6 , highlighted in Fig. 8, shows that neither free energy basin is connected via a monotonic “downhill” path to any of the free energy basins associated with the various phases of crystalline ice, which are expected to occur at much higher values of $Q_6 \simeq 0.5$. The properties of the phases associated with the two basins shown in Fig. 7(b) are, therefore, consistent with two distinct liquids, the LDL and HDL phases, predicted to occur in the ST2-RF model in earlier work.^{2,6,22}

If the two basins shown in Fig. 7(b) are consistent with a LLPT between LDL and HDL phases, then increasing the pressure at constant T should cause the LDL basin to disappear, and decreasing the pressure should cause the HDL basin to disappear, as both phases reach the respective spinodal limits that bracket the coexistence curve (see Fig. 1). This is illustrated in Figs. 7(a) and 7(c). At $P = 195$ MPa, only the LDL basin remains, while at $P = 230$ MPa only the HDL basin is observed.

We note that at $T = 240$ K, the pressure range found here that corresponds to the region between the HDL and LDL spinodals appears to be shifted downward by about 10 MPa relative to the thermodynamic features shown in Fig. 1.

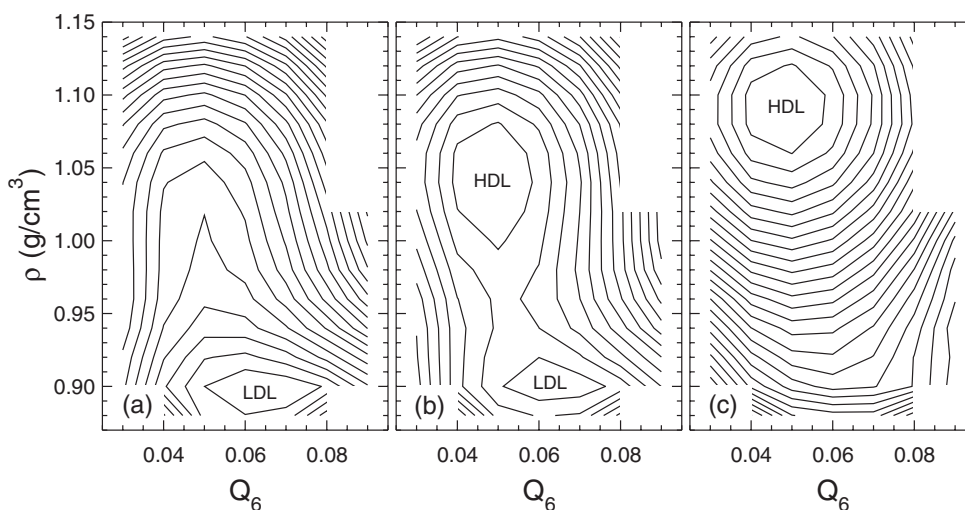


FIG. 7. Contour plots of $F(\rho, Q_6)$ at $T = 240$ K for (a) $P = 195$ MPa, (b) $P = 204.5$ MPa, and (c) $P = 230$ MPa. To evaluate these surfaces, we have coarse-grained the plane of ρ and Q_6 into rectangular cells of dimensions $\Delta\rho = 0.02$ g/cm³ and $\Delta Q_6 = 0.01$. Data from all series (K, L, and M) are combined and analyzed to obtain these plots. For each panel, contours are separated by $0.5kT$, and the error in F is $0.5kT$ or less. The lowest lying values of F in each plot are labelled LDL and/or HDL.

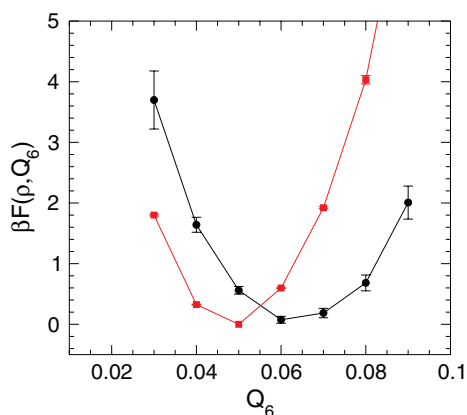


FIG. 8. Slices through the free energy surface $F(\rho, Q_6)$ for $T = 240$ K and $P = 204.5$ MPa [shown in Fig. 7(b)] as a function of Q_6 , passing through the minima of the LDL basin at $\rho = 0.90$ g/cm³ (circles), and the HDL basin at $\rho = 1.04$ g/cm³ (squares).

However, this difference is less than the error associated with the results in Fig. 1 for the location of the critical point and coexistence line. Considering that the features in Fig. 1 are based on an extrapolation of equation-of-state data from $N = 1728$ molecular dynamics simulations,^{6,24} and considering the possibility of differences due to finite-size effects when comparing with our $N = 216$ results, the agreement between the behavior observed here and that predicted in Fig. 1 is quite satisfactory.

Finally, in Fig. 9 we show the evolution of $\bar{F}(\rho)$ along a path in the T - P plane that approaches the vicinity of the predicted critical point in ST2-RF. Consistent with the occurrence of a line of first-order phase transitions terminating in a critical point, the two basins in $\bar{F}(\rho)$ are separated by a higher free energy barrier at lower T , which decreases in height, and then disappears, on approach to the critical point. Figure 9 also confirms that the density of the HDL phase varies significantly with T , whereas that of the LDL phase is comparatively

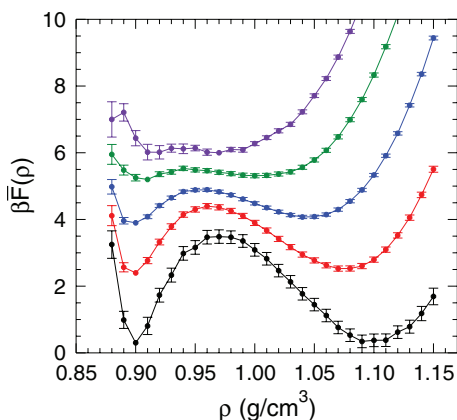


FIG. 9. Contracted free energy $\bar{F}(\rho)$ at several state points approaching the liquid-liquid critical point. From bottom to top, the state points are: $T = 230$ K and $P = 245$ MPa; $T = 235$ K and $P = 225$ MPa; $T = 240$ K and $P = 204.5$ MPa; $T = 245$ K and $P = 184$ MPa; and $T = 250$ K and $P = 164$ MPa. Each curve has been shifted by an arbitrary constant to facilitate comparison. The combined data from all series (K, L, and M) are analyzed to obtain each curve.

insensitive to changes in T . This observation is consistent with previous studies of the free energy of ST2 water that have observed distinct HDL and LDL basins.^{19,20,22}

V. DISCUSSION

In summary, for the ST2-RF model, we find two distinct basins in the free energy surface $F(\rho, Q_6)$, differing in density, but both occurring at low values of Q_6 , assuring that they correspond to disordered thermodynamic phases. Furthermore, our results for the structural relaxation times demonstrate that both basins correspond to equilibrated metastable liquid phases. These observations, and the dependence of the shape and position of the basins as a function of T and P are entirely consistent with the occurrence of a LLPT in the ST2-RF model of water, as described in previous work.^{2,5,6,22,23} Our results are also consistent with those of Liu and co-workers^{19,20} for the ST2 model using an Ewald treatment of the electrostatics. Our results are qualitatively different from the behavior of the ST2 system reported by Limmer and Chandler,¹⁶ and also are not consistent with their proposal that all the behavior previously ascribed to a LLPT in water-like models is in fact associated with the liquid-to-crystal transition.

We note that Limmer and Chandler²⁷ have argued that the observation of two liquid basins in $F(\rho, Q_6)$ could arise as an artifact of restricting the sampling to low values of Q_6 ; see Fig. 9 of Ref. 27 and the accompanying discussion. Limmer and Chandler²⁷ note that their own data for $\bar{F}(\rho)$ “exhibits an inflection or slight minimum” for low values of Q_6^{\max} , but that this shoulder in the curve merges into the minimum associated with the crystal basin for larger values of Q_6^{\max} . From this behavior, they conclude that although the shoulder observed for small Q_6^{\max} “could be confused with a second liquid basin,” it is in fact “due to the barrier separating liquid from crystal.”

We disagree with this interpretation of the data. We refer the reader to the bottom right-hand panel of Fig. 9 of Ref. 27, which shows the free energy surface upon which the above analysis of Limmer and Chandler²⁷ is based. In this free energy surface, the liquid basin is clearly distinct from the crystal basin, in the sense that any path connecting the minima of these two basins must pass over a barrier of at least $23kT$. The shoulder in the free energy surface noted by Limmer and Chandler²⁷ occurs deep inside the liquid basin (near $\rho = 0.92$ g/cm³ and $Q_6 = 0.08$), and is well separated from the barrier that defines the boundary between the liquid and crystal basins (near $Q_6 = 0.27$). Hence, any path leading from the shoulder to the crystal basin must go “uphill” in free energy at some point along the path. The shoulder thus cannot be understood as an extension of the crystal basin into the low- Q_6 regime. When $\bar{F}(\rho)$ is plotted for different Q_6^{\max} , the shoulder and the crystal minimum become superimposed on one another because they happen to occur at similar densities; however, this is not a basis for concluding that these two features must be associated with the same (crystalline) free energy basin.

To conclude, we emphasize that not all models of water exhibit a LLPT. For example, the mW model seems to be a case in which a LLPT, which otherwise might occur, becomes

unobservable due to the loss of stability of the supercooled liquid with respect to crystal nucleation.^{16,28,29} Whether or not a LLPT occurs in a given water model, and indeed in real water itself, may depend sensitively on the details of the intermolecular interaction. For real water, it remains for experiments to determine conclusively if a LLPT can be observed, for example, by manipulating the rate of ice crystallization in the supercooled regime by exploiting nano-confinement or external fields. Nonetheless, the results presented here provide clear evidence that a LLPT does occur in simulations of the ST2-RF model of water, and confirm the conclusions drawn in previous studies of this model regarding the existence of a LLPT.

ACKNOWLEDGMENTS

P.H.P. thanks Natural Sciences and Engineering Research Council (Canada) (NSERC) and the CRC program for support. F.S. thanks ERC-PATCHYCOLLOIDS. Computational resources were provided by ACEnet. We are grateful to P. G. Debenedetti, Y. Liu, J. C. Palmer, and T. Panagiotopoulos for informative discussions and for sharing their results in advance of publication. We also thank S. McGibbon-Gardner for useful discussions. Without implying their agreement with our methods or conclusions, we also thank D. Chandler and D. Limmer for discussions and for sharing their results in advance of publication.

¹F. H. Stillinger and A. Rahman, *J. Chem. Phys.* **60**, 1545 (1974).

²P. H. Poole, F. Sciortino, U. Essmann, and H. E. Stanley, *Nature (London)* **360**, 324 (1992).

³O. Mishima and H. E. Stanley, *Nature (London)* **396**, 329 (1998).

⁴P. G. Debenedetti, *J. Phys.: Condens. Matter* **15**, R1669 (2003).

⁵S. Harrington, R. Zhang, P. H. Poole, F. Sciortino, and H. Stanley, *Phys. Rev. Lett.* **78**, 2409 (1997).

⁶P. H. Poole, I. Saika-Voivod, and F. Sciortino, *J. Phys.: Condens. Matter* **17**, L431 (2005).

⁷D. Paschek, *Phys. Rev. Lett.* **94**, 217802 (2005).

⁸S. Sastry and C. A. Angell, *Nature Mater.* **2**, 739 (2003).

⁹V. V. Vasisht, S. Saw, and S. Sastry, *Nat. Phys.* **7**, 549 (2011).

¹⁰J. L. F. Abascal and C. Vega, *J. Chem. Phys.* **133**, 234502 (2010).

¹¹P. Gallo and F. Sciortino, *Phys. Rev. Lett.* **109**, 177801 (2012).

¹²C. Huang *et al.*, *Proc. Natl. Acad. Sci. U.S.A.* **106**, 15214 (2009).

¹³G. N. I. Clark *et al.*, *Proc. Natl. Acad. Sci. U.S.A.* **107**, 14003 (2010).

¹⁴Y. Zhang *et al.*, *Proc. Natl. Acad. Sci. U.S.A.* **108**, 12206 (2011).

¹⁵K. Winkel, E. Mayer, and T. Loerting, *J. Phys. Chem. B* **115**, 14141 (2011).

¹⁶D. T. Limmer and D. Chandler, *J. Chem. Phys.* **135**, 134503 (2011).

¹⁷V. Molinero and E. B. Moore, *J. Phys. Chem. B* **113**, 4008 (2009).

¹⁸P. J. Steinhardt, D. R. Nelson, and M. Ronchetti, *Phys. Rev. B* **28**, 784 (1983).

¹⁹Y. Liu, J. C. Palmer, A. Z. Panagiotopoulos, and P. G. Debenedetti, *J. Chem. Phys.* **137**, 214505 (2012).

²⁰Y. Liu, A. Z. Panagiotopoulos, and P. G. Debenedetti, *J. Chem. Phys.* **131**, 104508 (2009).

²¹O. Steinhauser, *Mol. Phys.* **45**, 335 (1982).

²²F. Sciortino, I. Saika-Voivod, and P. H. Poole, *Phys. Chem. Chem. Phys.* **13**, 19759 (2011).

²³T. A. Kesselring, G. Franzese, S. V. Buldyrev, H. J. Herrmann, and H. E. Stanley, *Sci. Rep.* **2**, 474 (2012).

²⁴M. J. Cuthbertson and P. H. Poole, *Phys. Rev. Lett.* **106**, 115706 (2011).

²⁵P. H. Poole, S. R. Becker, F. Sciortino, and F. W. Starr, *J. Phys. Chem. B* **115**, 14176 (2011).

²⁶M. R. Shirts and J. D. Chodera, *J. Chem. Phys.* **129**, 124105 (2008). We use the “pymbar-2.0beta” implementation of the MBAR method, see <https://simtk.org/home/pymbar>.

²⁷D. T. Limmer and D. Chandler, e-print [arXiv:1107.0337v2](https://arxiv.org/abs/1107.0337v2).

²⁸E. B. Moore and V. Molinero, *Nature (London)* **479**, 506 (2011).

²⁹V. Molinero, S. Sastry, and C. A. Angell, *Phys. Rev. Lett.* **97**, 075701 (2006).